Solar Energy 264 (2023) 112075

Contents lists available at ScienceDirect

Solar Energy

journal homepage: www.elsevier.com/locate/solener

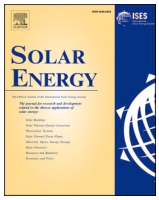

Innovative integrated solar combined cycle: Enhancing dispatchability with a partial recuperative gas turbine and supercritical CO_2 bottoming cycle, coupled with an ORC

José Ignacio Linares [a,*], Eva Arenas [a,b], Alexis Cantizano [a,b], Maria José Montes [c], Antonio José Rovira [c], José Porras [a], José Rubén Pérez-Domínguez [a]

[a] ICAI School of Engineering, Comillas Pontifical University, Alberto Aguilera 25, 28015 Madrid, Spain
[b] Institute for Research in Technology, Comillas Pontifical University, Santa Cruz de Marcenado 26, 28015 Madrid, Spain
[c] Department of Energy Engineering, Universidad Nacional de Educación a Distancia (UNED), Juan del Rosal 12, 28040 Madrid, Spain

ARTICLE INFO

Keywords:
Recuperative gas turbine
CSP
Combined cycle
supercritical CO_2 power cycle

ABSTRACT

Concentrating solar power is crucial in the future energy mix due to its ability to integrate thermal energy storage, thus providing dispatchability. One way to address the current high costs of this technology is by using higher temperatures, which can, however, lead to issues with heat transfer fluids and storage. A promising integrated solar combined cycle is here proposed to solve that current major issue. A partially recuperated gas turbine is coupled to a solar tower system using a Brayton supercritical CO_2 power cycle, which recovers heat at two temperature levels. An Organic Rankine Cycle is also used to exploit the low-temperature flue gases. The performance at the design point is assessed under different solar contributions. The modulation of the thermal duty in the gas turbine recuperator allows reaching a nearly constant power production in the plant (180 MWe): 56 % coming from the gas turbine, 39 % from the CO_2 power cycle, and 5 % from the ORC. The global efficiency achieved is 57.2 %. Carbon dioxide emissions range from 236 g CO_2/kWhe (86 g CH_4/kWhe are consumed) with the maximum solar contribution to 346 g CO_2/kWhe (126 g CH_4/kWh are consumed) with no solar contribution.

1. Introduction

Many countries are paying attention to Concentrated Solar Power (CSP) technology [1] because it will play a significant role in the grid management of the future energy mix. Firstly, CSP can be considered a dispatchable renewable energy due to its ability to store large-scale thermal energy and secondly, because the inertia of the generator contributes to the grid frequency stability. However, a critical bottleneck for the deployment of CSP is its current high-levelized cost of electricity (LCOE) [2]. In addition, the oversizing of the solar field to store the surplus of thermal energy shares a relevant part of the capital expenditure (CAPEX), despite being one of the strengths of this technology (dispatchability) [3]. According to the International Renewable Energy Agency (IRENA), the world-installed CSP power has increased from 2010 to the present, with a reduction in the LCOE from 346 $/MWh to 182 $/MWh [4]. Unfortunately, such cost is still far from the 60 $/MWh goal established by the SunShot Initiative of the US Department of Energy [5]. The LCOE reduction during the last decade has been mainly motivated by a decrease in the solar field cost (responsible for the 40 % of the investment costs) due to the scale economy. A second approach to cost reduction is to increase the system's efficiency, which leads to increase the turbine inlet temperature. The U.S. Department of Energy (DOE), through the Gen3 CSP Roadmap [6] has established central solar receiver (CRS) power plants with Brayton supercritical CO_2 power cycle (S-CO2) as the standard for the next generation of concentrated solar power plants, aiming for turbine inlet temperatures exceeding 700 °C. To achieve this, three potential pathways have been selected, depending on the type of thermal carrier in the receiver: molten salt, particles or gaseous medium. Each of these pathways faces different challenges associated with the high temperature objective. Current molten salts used in CSP (both as an energy carrier and storage fluid) can not withstand such temperature, being precise to replace them by ternary salts, which presents new challenges; in the case of particle-based systems, there is limited experience with high temperatures and pressures required by S-CO2, in addition to the challenges associated with heating particles using concentrated sunlight; finally, the gas-phase pathway requires a high-pressure receiver with an indirect storage option.

* Corresponding author.
E-mail address: linares@comillas.edu (J.I. Linares).

https://doi.org/10.1016/j.solener.2023.112075
Received 30 May 2023; Received in revised form 15 September 2023; Accepted 27 September 2023
Available online 4 October 2023
0038-092X/© 2023 The Author(s). Published by Elsevier Ltd on behalf of International Solar Energy Society. This is an open access article under the CC BY-NC-ND license (http://creativecommons.org/licenses/by-nc-nd/4.0/).

Nomenclature

Acronyms

AC	Air Compressor (Gas turbine block)
AdInCCSol	Advanced Integration of Combined Cycles in Solar thermal power plants
ASME	American Society of Mechanical Engineers
C	Compressor (S-CO2 block)
CAPEX	Capital Expenditure
CC	Combustion Chamber (Gas turbine block)
CHE	Compact Heat Exchanger
COND	Condenser (ORC block)
CRS	Central Receiver System (S-CO2 block)
CSP	Concentrated Solar Power
DOE	US Department of Energy
EES	Engineering Equation Solver
FGT	Flue Gases Turbine (Gas turbine block)
G-HTR	Gas High-Temperature Recuperator (S-CO2 block)
G-REC	Gas turbine Recuperator (Gas turbine block)
GWP	Global Warming Potential
HLHX	Heating Loop Heat eXchanger (S-CO2 block)
HRSG	Heat Recovery Steam Generator
HT	High Temperature
HTHR	High-Temperature Heat Recovery (S-CO2 block)
HTR	High-Temperature Recuperator (S-CO2 block)
IRENA	International Renewable Energy Agency
ISCC	Integrated Solar Combined Cycle
IT	Intermediate Temperature
ITHR	Intermediate Temperature Heat Recovery (S-CO2 block)
ITLP	Intermediate Temperature Loop Pump (S-CO2 block)
LCOE	Levelized Cost of Electricity
LTHR	Low-Temperature Heat Recovery (ORC block)
LTR	Low-Temperature Recuperator (S-CO2 block)
NREL	National Renewable Laboratory
ODP	Ozone Depletion Potential
O-P	Pump (ORC block)
ORC	Organic Rankine Cycle
O-REC	Recuperator (ORC block)
O-T	Turbine (ORC block)
PC	Precooler (S-CO2 block)
PCHE	Printed Circuit Heat Exchanger
PTC	Parabolic Trough Collector
R600	N-butane
S-CO2	Brayton supercritical CO_2 power cycle
S-HTR	Solar High-Temperature Recuperator (S-CO2 block)
T	Turbine (S-CO2 block)
TES	Thermal Energy Storage

Symbols

g	specific gas consumption
h	specific enthalpy
H	height
$\dot{m}$	mass flow rate
$\dot{Q}$	thermal power
UA	thermal conductance
w	specific power
W	width

Subscripts

AC	air compressor
c	compressor, cold
CC	combyned cycle
CCH	combustion chamber
FGT	flue gases turbine
GT	gas turbine
h	hot
i	inlet
$ITLP$	intermediate temperature loop pump (S-CO2 block)
N	nominal
o	outlet
$O\text{-}P$	pump (ORC block)
ORC	organic Rankine cycle
$O\text{-}T$	turbine (ORC block)
p	pump
s	isentropic
$S\text{-}CO2$	Brayton supercritical CO_2 power cycle
T	turbine

Brayton supercritical CO_2 power cycles [7] exhibit higher efficiencies than Rankine cycles within the temperature range commonly present in CSP. This higher efficiency can be attributed to two primary factors. On the one hand, the ability of S-CO2 to recuperate heat from the turbine outlet to preheat the compressor outlet. On the other hand, the compressor suction conditions (75 bar to 90 bar and 35 °C to 50 °C) are very close to the CO_2 critical point (73.8 bar and 31 °C), highly increasing its density. Thus, the compressor consumption is reduced, enabling high efficiencies with turbine inlet temperatures lower than those used in gas turbines (open Brayton cycle with air). In fact, efficiency ranges from 40 % to 50 % with turbine inlet temperatures from 500 °C to 700 °C. Basic and simple recuperative layouts of transcritical S-CO2 have been proposed by Sajwan et al. [8] for waste heat recovery in reciprocating engines with turbine inlet temperatures below 500 °C. Nevertheless, the operation of CO_2 close to the critical point makes it difficult to yield the maximum recuperative potential, although this is overcome by splitting the recuperator into two units (low-temperature recuperator, LTR, and high-temperature recuperator, HTR), known as re-compression S-CO2 cycle. In this layout, the LTR recuperator operates at low temperatures and with two different mass flow rates in each stream. This is due to the higher specific heat of the higher-pressure stream, requiring a lower mass flow rate. By carefully selecting an appropriate mass flow rate split ratio, the LTR recuperator can be balanced: part of the low-pressure stream is not cooled when it leaves the recuperator and is conducted to an auxiliary compressor (that is the reason to designate this layout as “re-compression”) whose output is mixed with the cold stream leaving the LTR recuperator, which was compressed in the main compressor once it was cooled down.

Research on S-CO2 in Concentrated Solar Power (CSP) has emerged relatively recently. Turchi et al. [9] proposed the use of a re-compression layout with modular towers in a central receiver system power plant (CRS). In this study, authors took advantage of the compact size of S-CO2, integrating the power block in the tower using a direct cycle layout. Later, in 2014, the National Renewable Energy Laboratory (NREL) [10] assessed the efficiency of the plant and associated turbomachinery at a scaled size according to actual CSP projects to promote S-CO2 at a commercial level. Crespi et al. [11] performed a general evaluation of S-CO2 for power generation, whereas Wang et al. [12] identified and analyzed six S-CO2 layouts indirectly coupled to a CRS working with molten salts. They concluded that there is not any layout clearly better than others, being necessary to consider the specific operation conditions, and especially the annual performance. When molten salts are used as the working fluid in CRSs, the primary heat exchanger plays a key role. Printed circuit heat exchangers (PCHE) are commonly proposed for S-CO2 power cycles due to their ability to withstand the high pressures involved in these cycles. However, their

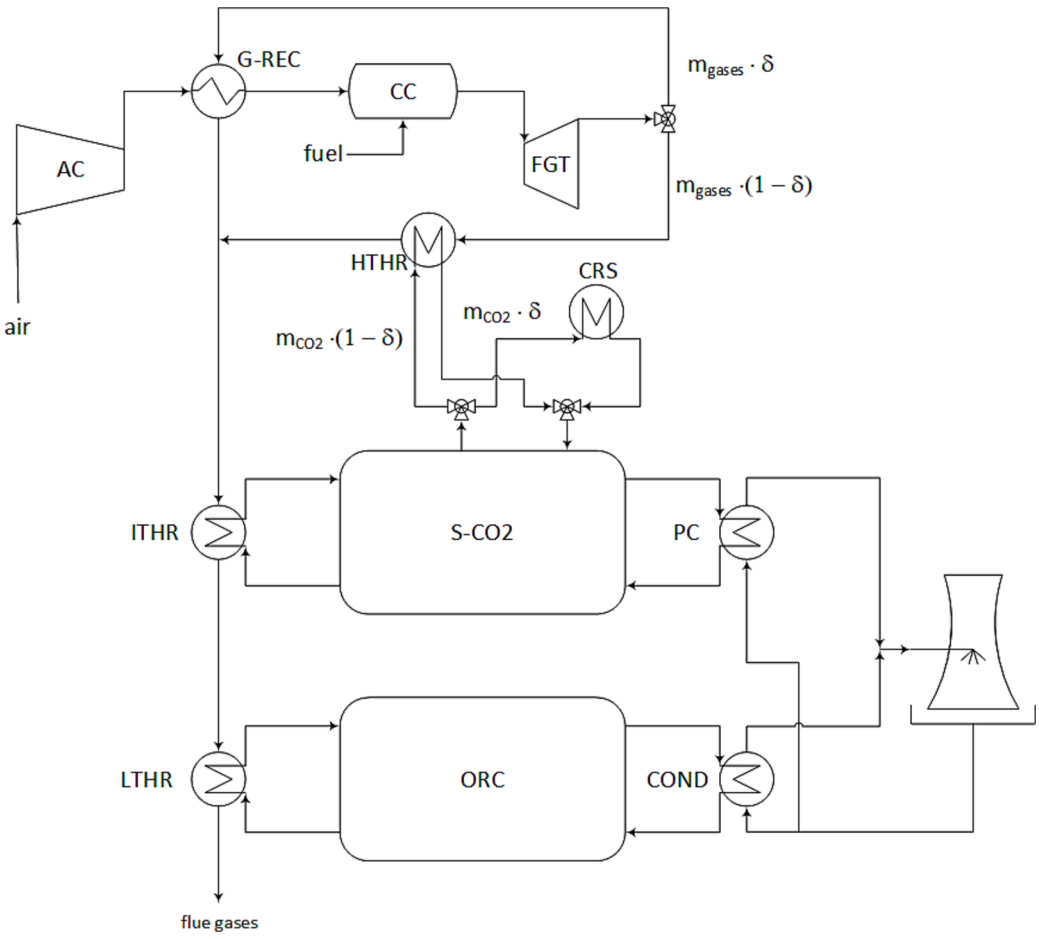

Fig. 1. Conceptual diagram of the proposed system.

narrow channels make it difficult to use them as the primary heat exchangers in a molten salts/CO_2 configuration [13]. Montes et al. [14] proposed a modified PCHE with wider channels in the salt stream and another design based on a honeycomb structure with the molten salt flowing across wide circular channels [15]. Finally, Linares et al. [16] proposed the use of a shell and tube heat exchanger with the molten salt flowing across the shell. The pressure issue was solved by relocating the primary heat exchange downstream of the turbine in a novel S-CO2 layout.

Although indirect coupling (one fluid in the receiver and another working fluid in the power cycle) is the most common arrangement in CSP, direct coupling has also been proposed, involving the use of CO_2 in the receiver and in the S-CO2 power cycle. However, this has always been limited to CRS plants, as the high pressure of the S-CO2 cycle make it difficult its use in parabolic trough collectors [9]. Although indirect two-tank molten salts thermal energy storage is the usual solution in direct-coupled proposals [9], other solutions are possible, like the one explored by Johnson et al. [17], based on a packed bed storage.

In a direct coupling configuration, CO_2 flows inside the central receiver. Li et al. [18] conducted a review of compact heat exchangers and considered their integration into pressurized solar receivers. One of the first proposed central receivers with supercritical CO_2 was based on the external tubular receiver concept [19]. This design was intended to heat the air to 800 °C at 5 to 7 bar and is being considered to operate with CO_2 at 700 °C and 200 bar once challenges related to high pressure and heat transfer under supercritical conditions are overcome. Besarati et al. [20] used the compact heat exchanger (CHE) concept in a cavity receiver for supercritical CO_2. The receiver consisted of several plates joined by diffusion, with rectangular fins between them. The authors investigated its optimal geometry. The NREL has also investigated the application of CHEs, presenting two concepts for supercritical CO_2 central receivers [21]. The first design is a cavity receiver, whereas the second is a surrounded external receiver. In both designs, CO_2 flows through a compact structure of two attached plates with a wavy fin structure between them. Montes et al. [22] have proposed a novel design of a microchannel central receiver consisting of a radial arrangement of vertical absorber panels that converge on the central axis of the tower, analysing in [23] its application to different S-CO2 cycles in indirect coupling and re-compression S-CO2 in direct coupling.

Some authors have explored the use of an organic Rankine cycle (ORC) to recover the rejected heat from the S-CO2, thereby constituting a combined cycle. Song et al. [24] carried out a parametric optimization of such a combined cycle, while Singh and Mishra [25] analyzed the use of a PTC as a heat source for the system. In both cases, re-compression was not included in the S-CO2 cycle. Hou et al. [26] optimized a combined S-CO2 re-compression cycle (750 °C as turbine inlet temperature) with a recuperative ORC using a zeotropic mixture fluid.

As mentioned earlier, the dispatchability of the CSP is usually addressed through thermal energy storage (TES) fed by an oversized solar field. There are several TES systems: thermocline tank, two-tank with a high-density fluid (e.g., molten salts) or particles [27], phase change materials and solid storage in bedrocks [28]. However, another way to solve dispatchability is to arrange a hybrid layout with auxiliary boilers fed by natural gas or biomass [29]. This configuration enables an increase in the turbine inlet temperature, thus enhancing the efficiency. If biomass is used as fuel, the renewable feature of the system is maintained.

Central receiver systems can be integrated into a combined cycle in

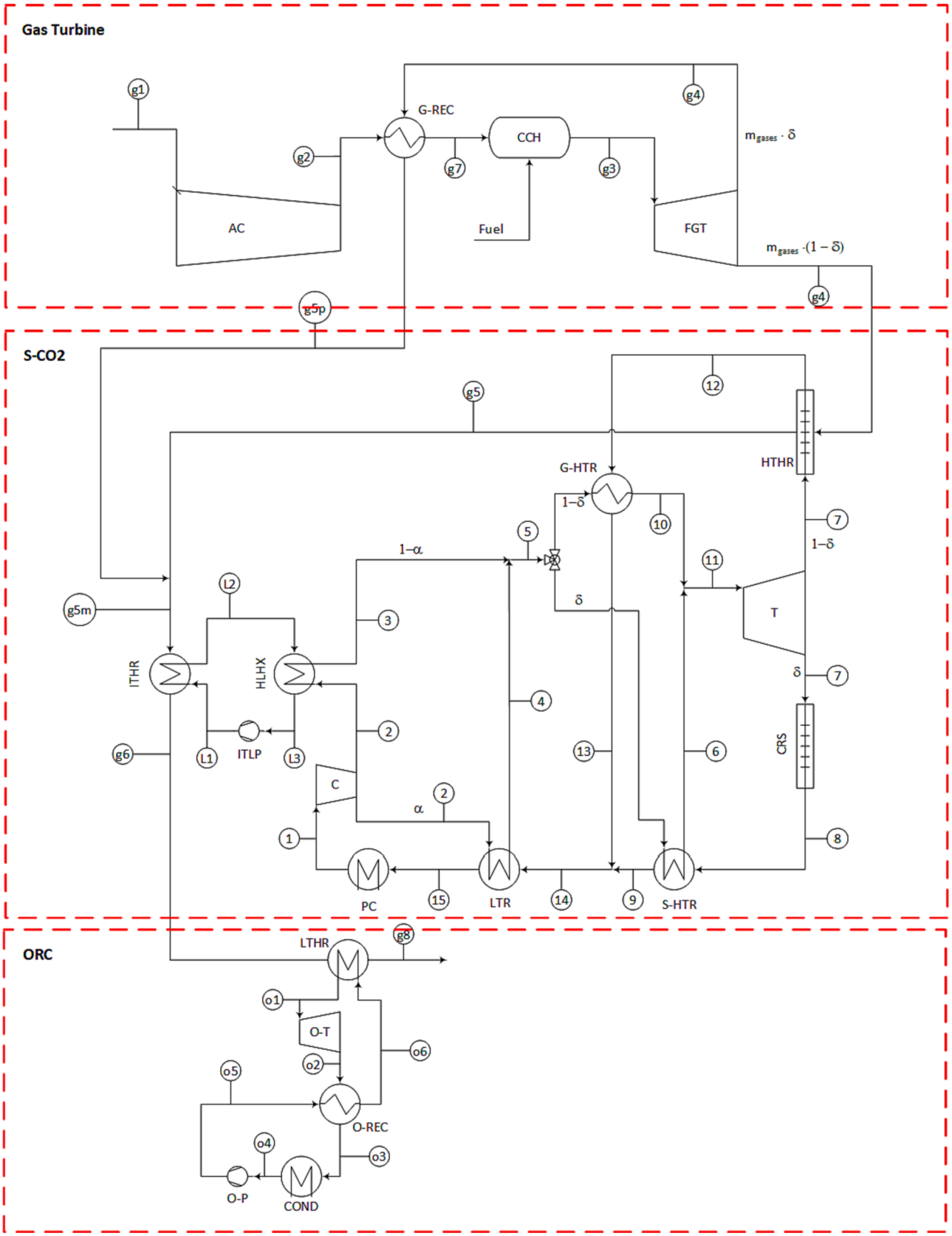

Fig. 2. Layout of the proposed power plant with all the system components.

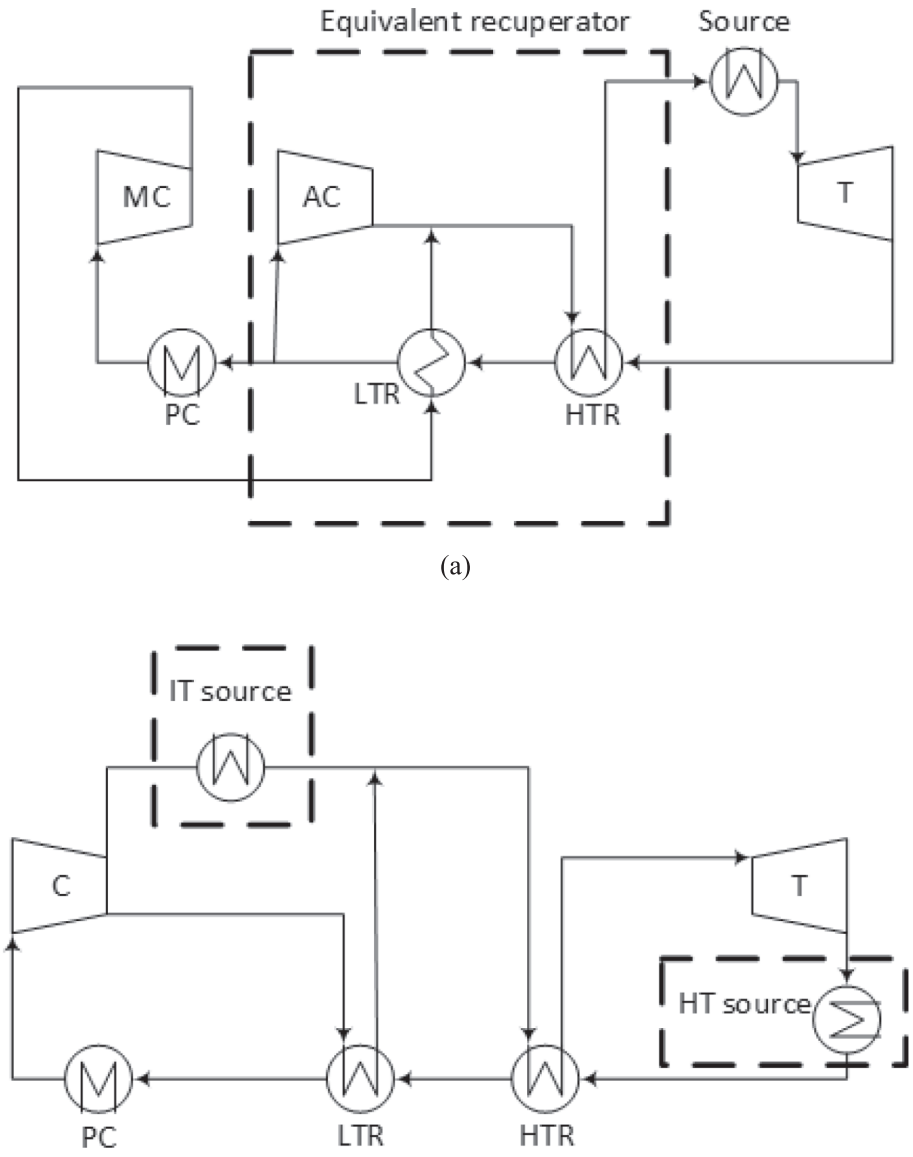

Fig. 3. Recompression layouts: (a) Classical; (b) Modified.

several ways, allowing beneficial synergies between fossil fuel and solar technologies. Thus, solar contribution can compensate for the production reduction typically observed in conventional combined cycles during periods of high solar radiation, due to the higher ambient temperature [30]. The integration can be done into the Rankine bottom cycle, commonly referred to as Integrated Solar Combined Cycle (ISCC), or into the gas turbine. In the former, early studies proposed solar energy to be incorporated in parallel to the heat recovery steam generator (HRSG) [31]. However, Kane et al. [32] concluded that this scheme was only economically feasible if subsidies were provided. Economic feasibility and production costs were later analyzed by Dersch et al. [33] and Franchini et al. [34]. Parabolic trough collectors were the most common technology, as it is seen in Sharma et al. [35], who studied the integration of this type of solar field with a combined cycle used in trigeneration mode in 10 to 50 MW scale by means of energy and exergy balance. Other solar concentration technologies have also been considered, such as the central receiver [36] or the linear Fresnel [37]. Khandelwal et al. [38] have analysed the integration of linear Fresnel and latent heat cascade storage system, assessing the performance at full load and partial load of gas turbine with different heat transfer fluids in both receiver and storage. Regarding the solar integration into the gas turbine, Amelio et al. [39] proposed to heat up the combustion air with parabolic trough collectors. This idea was also proposed by Duan et al. [40], but preheating the water for the HRSG with the air leaving the compressor. Central receivers, preheating the combustion air, were also proposed in [41].

The use of recuperative gas turbines in the ISCC systems has been explored, aiming to improve the efficiency. However, the results do not support the inclusion of this technology in commercial plants [42]. Liu et al. [43] pursued this approach but with partial recuperation. Partial recuperation was also explored by Rovira et al. [44], looking for modulating the recuperation in the gas turbine based on the solar contribution in the HRSG.

The present work is framed in the project AdInCCSol (Advanced Integration of Combined Cycles in Solar thermal power plants), where four different solar technologies and power cycles are being analyzed [45]. The current proposal is an ISCC consisting of a partial recuperative gas turbine where the traditional Rankine bottoming cycle has been

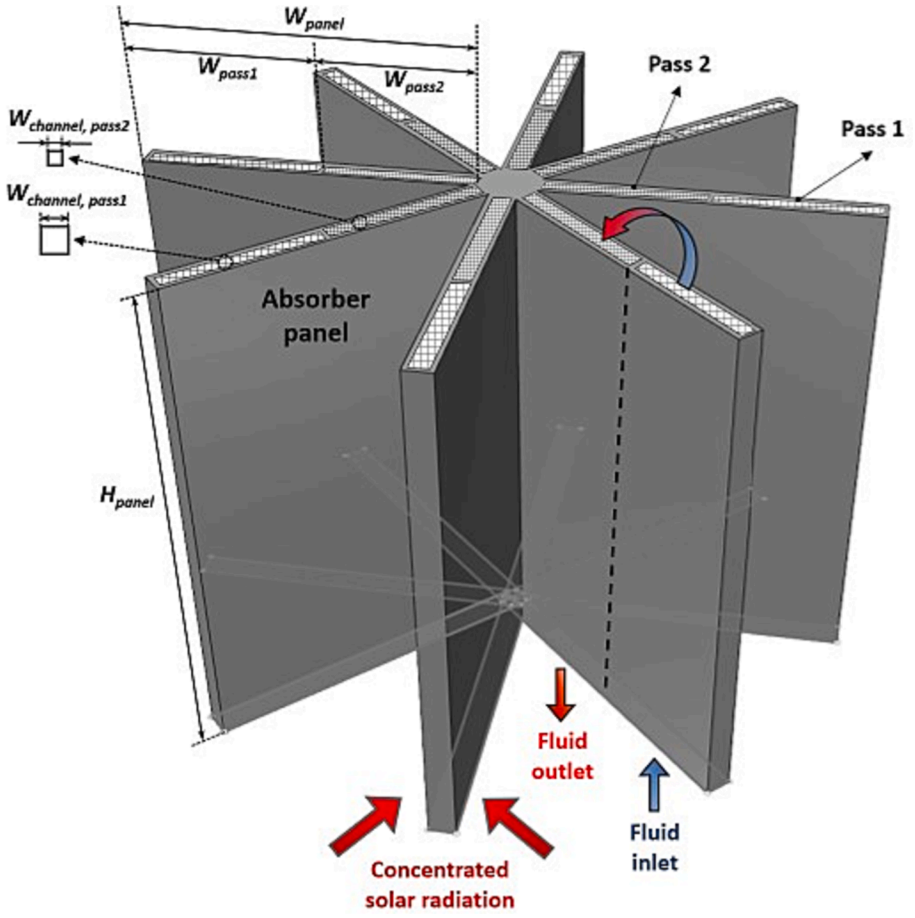

Fig. 4. Schematic of the microchannel central solar receiver for supercritical CO_2 analysed in this work.

Table 1
Boundary conditions at gas turbine.

Variable	Value	Reference
AC inlet temperature [°C]	15	[53]
AC inlet pressure [bar]	1	[53]
AC isentropic efficiency [%]	85	[54]
CCH fuel inlet temperature [°C]	25	
FGT inlet temperature [°C]	1,500	
FGT outlet temperature (FGT) [°C]	950	
FGT isentropic efficiency [%]	90	[54]

Table 2
Boundary conditions at flue gases stream.

Variable	Value	Reference
Solar contribution [%]	0–100	
Design temperature approach at HTHR [°C]	30	[16]
Flue gases outlet design temperature of LTHR [°C]	115	

replaced by a Brayton supercritical CO_2 power cycle. Fig. 1 shows the conceptual diagram. In this system, a fraction of the flue gases by-passes the gas turbine recuperator (G-REC) and provides heat to the S-CO2 cycle through the high-temperature heat recovery heat exchanger (HTHR), in parallel with the CRS. This fraction is modulated according to the solar contribution. This stream is mixed with the remaining flue gases, upon leaving the gas turbine recuperator, and supplies intermediate-temperature heat to the S-CO2 cycle through the intermediate-temperature heat recovery heat exchanger (ITHR). In this

Table 3
Boundary conditions at organic Rankine cycle.

Variable	Value	Reference
O-P inlet temperature [°C]	35	
O-P isentropic efficiency [%]	75	[55]
O-T inlet design pressure [bar]	50	
O-T inlet design temperature [°C]	200	
O-T isentropic efficiency [%]	80	[55]
Condenser cooling water inlet temperature [°C]	25	
O-REC design temperature approach [°C]	10	

Table 4
Boundary conditions at Brayton supercritical CO_2 power cycle.

Variable	Value	Reference
C inlet temperature [°C]	35	
C inlet pressure [bar]	85	
C outlet pressure [bar]	300	
C isentropic efficiency [%]	87	[16]
T isentropic efficiency [%]	92	[16]
ITLP isentropic efficiency [%]	75	[16]
G-HTR and S-HTR inlet temperature of low-pressure streams [°C]	700	
G-HTR and S-HTR design temperature approach [°C]	10	[16]
LTR design temperature approach [°C]	5	[16]
Pressure drop of CO_2 stream at heat exchangers [bar]	0.4	[16]
PC cooling water inlet temperature [°C]	25	

Table 5
Design point conditions of the gas turbine turbomachines ($\delta = 0$).

	Point	p [bar]	T [°C]	$\dot{m}$[kg/s]	$\dot{W}$[kW]
Compressor (AC)	g1	1	15	195.1	48,333
	g2	6.752	257		
Turbine (FGT)	g3	6.752	1,500	201.5	148,333
	g4	1	950		

Table 6
Design point conditions of the gas turbine recuperator (G-REC) ($\delta = 1$).

	Point	p [bar]	T [°C]	$\dot{m}$[kg/s]	$\dot{Q}$[kW]
Cold stream	g2	6.752	257	195.1	96,574
	g7	6.752	705.7		
Hot stream	g4	1	940.1	199.5	
	g5p	1	539.5		

Table 7
Design point conditions of the turbomachines of the bottoming cycles ($\delta = 0$).

	Point	p [bar]	T [°C]	$\dot{m}$[kg/s]	$\dot{W}$[kW]
Compressor CO_2 (C)	1	85	35	443.9	11,761
	2	300	72.55		
Turbine CO_2 (T)	11	299.2	674.1	443.9	84,514
	7	86.6	510.4		
Heating loop pump CO_2 (ITLP)	L3	85	77.6	120.7	31.9
	L1	85.8	78.3		
Turbine n-butane (O-T)	o1	50	198.9	106.7	11,305
	o2	3.29	108.4		
Pump n-butane (O-P)	o4	3.29	35	106.7	1,186
	o5	50	39.4		

way, the thermal effect of the auxiliary compressor is effectively replaced. Finally, the low-temperature heat remaining in the flue gases stream is recovered in an ORC power cycle through the low-temperature heat recovery heat exchanger (LTHR). The modulation of the gas turbine recuperator according to the solar radiation enables a nearly constant power output, constituting one of the novelties of the hybrid combined cycle proposed in this work. The integration of the solar tower system with the recuperative gas turbine allows to replace the thermal energy storage system usually employed at CSP to achieve dispatchability. Such storage systems face important challenges due to the future high turbine inlet temperature required in order to increase efficiency. Therefore, the current proposal provides a solution to this issue. Furthermore, since this storage system requires oversizing the solar field, a substantial reduction in CAPEX is expected. On the other hand, partial recuperation increases the capacity factor compared to a pure CSP plant, converting all solar hours (actual radiation) into equivalent hours (design radiation). Another novelty of this integration is adapting the S-CO2 power cycle to the different thermal sources imposed by the integration. In this sense, a recompression layout has been taken as a basis, but the heating supply has been relocated downstream of the turbine. This allows the use of CO_2 as the heat transfer fluid both in the solar receiver (direct cycle) and in the cross-flow heat exchanger that recovers the heat from the gas turbine flue gases, mainly because the CO_2 in these components operates at the

Table 9
Design point conditions of the thermal sources and sink heat exchangers of the bottoming cycles ($\delta = 0$).

		Point	p [bar]	T [°C]	$\dot{m}$[kg/s]	$\dot{Q}$[kW]
HTHR	Cold stream (CO_2)	7	86.6	510.4	443.9	102,785
		12	86.2	700		
	Hot stream (Flue gases)	g4	1	949.9	199.3	
		g5	1	540.3		
ITHR	Cold stream (CO_2)	L1	85.8	78.28	120.7	46,973
		L2	85.4	405		
	Hot stream (Flue gases)	g5m	1	539	201.5	
		g6	1	399.5		
HLHX	Cold stream (CO_2)	2	300	72.55	93.3	47,005
		3	299.6	400		
	Hot stream (CO_2)	L2	85.4	405	120.7	
		L3	85	77.55		
PC	Cold stream (Water)	Inlet	6	25	3685	77,037
		Outlet	5	30		
	Hot stream (CO_2)	15	85.4	77.55	443.9	
		1	85	35		
LTHR	Cold stream (n-butane)	o6	50	84	106.7	50,375
		o1	50	199		
	Hot stream (Flue gases)	g6	1	339.5	201.5	
		g8	1	114		
COND	Cold stream (Water)	Inlet	6	25	1926	40,256
		Outlet	5	30		
	Hot stream (n-butane)	o3	3.29	49.1	106.7	
		o4	3.29	35		

Table 8
Design point conditions of the recuperators of the bottoming cycles ($\delta = 0$).

		Point	p [bar]	T [°C]	$\dot{m}$[kg/s]	$\dot{Q}$[kW]
HTR	Cold stream (CO_2)	5	299.6	437.2	443.9	133,411
		10/6	299.2	674		
	Hot stream (CO_2)	12/8	86.2	700	443.9	
		13/9	85.8	452.2		
LTR	Cold stream (CO_2)	2	300	72.55	350.6	197,566
		4	299.6	447.1		
	Hot stream (CO_2)	14	85.8	452.1	443.9	
		15	85.4	77.55		
O-REC	Cold stream (n-butane)	o5	50	39.4	106.7	12,718
		o6	50	84.0		
	Hot stream (n-butane)	o2	3.29	108.4	106.7	
		o3	3.29	49.1		

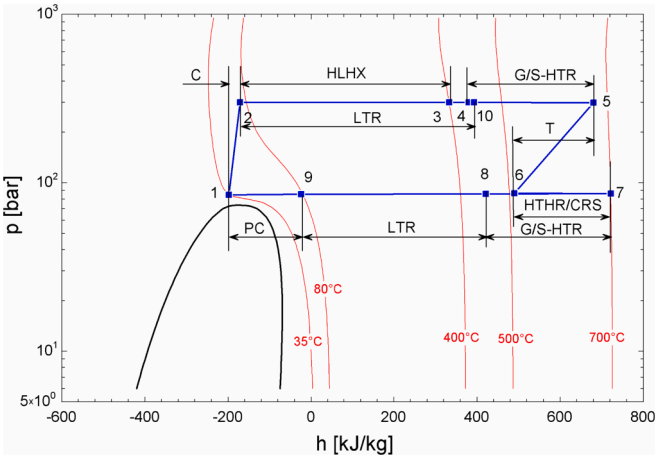

Fig. 5. P-h diagram of the S-CO2 power cycle. Numbers correspond to Fig. 5, where parallel twin components have been condensed.

lower pressure range of the cycle. This way to solve the heating supply issue comes from an original design by the authors [16] and enhances the efficiency by avoiding the use of intermediate loops. Finally, another variation included in the S-CO2 power cycle is the replacement of the auxiliary compressor by the intermediate-temperature heat supply downstream of the compressor once both flue gases streams have mixed.

2. Methodology

2.1. Layout

The plant layout is shown in Fig. 2, where the three main subsystems can be seen: the gas turbine cycle, the S-CO2 cycle and the ORC. Each subsystem constitutes an energy conversion system fed from different sources: primary energy (fuel in the gas turbine cycle), waste heat (flue gases from the gas turbine in the ORC) or a combination of both (flue gases from the gas turbine in parallel with solar radiation in the S-CO2 cycle). The thermal backbone of these subsystems is the flue-gases stream coming from the gas turbine, with three distinct temperature levels. Upon leaving the gas turbine, these gases represent the highest temperature source and provide heat to the S-CO2 cycle in the HTHR. The intermediate temperature source is a mixture of the flue gases leaving the G-REC and those leaving the HTHR. This mixed stream supplies heat to the S-CO2 cycle in the ITHR through an intermediate loop. Finally, the flue-gases stream leaving the ITHR serves as the low-temperature source, which is then recovered in the LTHR, feeding the ORC. Regarding the cold reservoir, the heat rejection is performed by the precooler (PC) in the S-CO2, and by the condenser (COND) in the ORC, both connected to a cooling tower.

The CRS, in parallel with the HTHR, represents the high-temperature source and feeds the S-CO2 cycle. In this sense, the proposed system does not include thermal energy storage to avoid the cost associated with oversizing the solar field and the potential issues associated with this system when the turbine inlet temperature is increased in order to reach higher efficiencies. Instead, dispatchability relies on support from the gas turbine, while an increase in capacity factor is achieved through the combination of the HTHR and the CRS in such a way that, when the solar radiation is high, the flue-gases stream sent to the HTHR is low, deriving the rest to the G-REC. Thus, this recuperator operates at different heat duties depending on the solar contribution. This type of recuperated gas turbine has been described as a "partially recuperated gas turbine" by authors in previous studies [46]. This modulation is characterized by the solar contribution factor (δ), which represents the fraction of CO_2 mass flow rate leaving the turbine (T) and collecting the solar radiation in the CRS. The remaining mass flow rate (1-δ) collects heat from the flue gases in the HTHR. This parameter also represents the splitting of the flue-gases mass flow rate leaving the FGT, where a fraction δ is directed to the G-REC and the rest (1-δ) to the HTHR. The mass flow rate through the G-REC increases with a higher solar contribution. Thus, this modulation enables the enhancement of the capacity factor by transforming all actual solar hours into equivalent hours. In other words, the system potencially maintains a constant power output throughout the solar hours, reducing the gas supply as solar radiation increases. If production is required during non-solar hours, the system behaves as a combined cycle (with S-CO2 instead of a Rankine cycle). However, it is important to note that the constancy in the power output is contingent on the air

Table 10
Geometrical parameters of the microchannel receiver.

Number of converging absorber panels	8
Panel width in pass 1 (W_{panel}) [m]	3.3
Panel height in pass 1 (H_{panel}) [m]	4.62
Width in pass 1 (W_{pass1}) [m]	1.38
Channel dimensions in pass 1 ($W_{channel,pass1} \times W_{channel,pass1}$) [mm × mm]	10 × 10
Panel width in pass 2 (W_{panel}) [m]	6
Panel height in pass 2 (H_{panel}) [m]	1.92
Width in pass 2 (W_{pass2}) [m]	5 × 5
Channel dimensions in pass 2 ($W_{channel,pass2} \times W_{channel,pass2}$) [mm × mm]	6

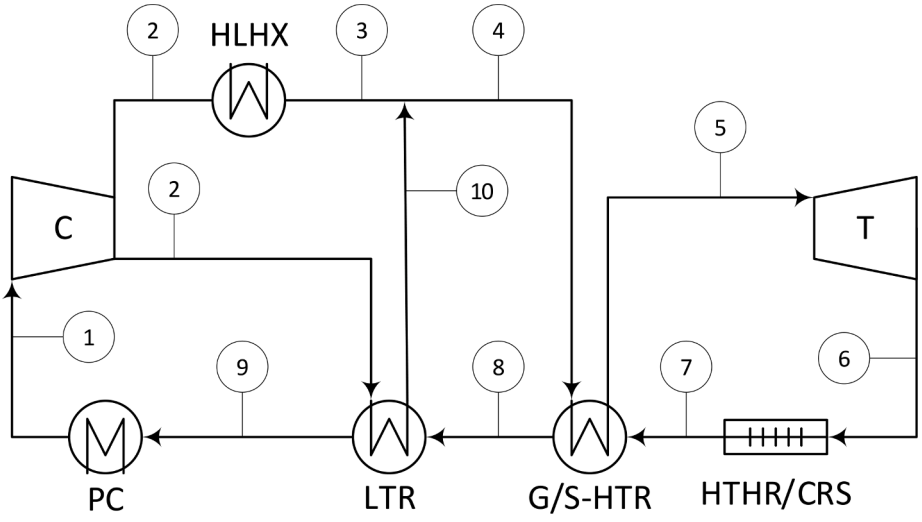

Fig. 6. Simplified version of the S-CO2 layout shown in Fig. 1. Parallel twin components have been condensed into single units for the sake of simplicity.

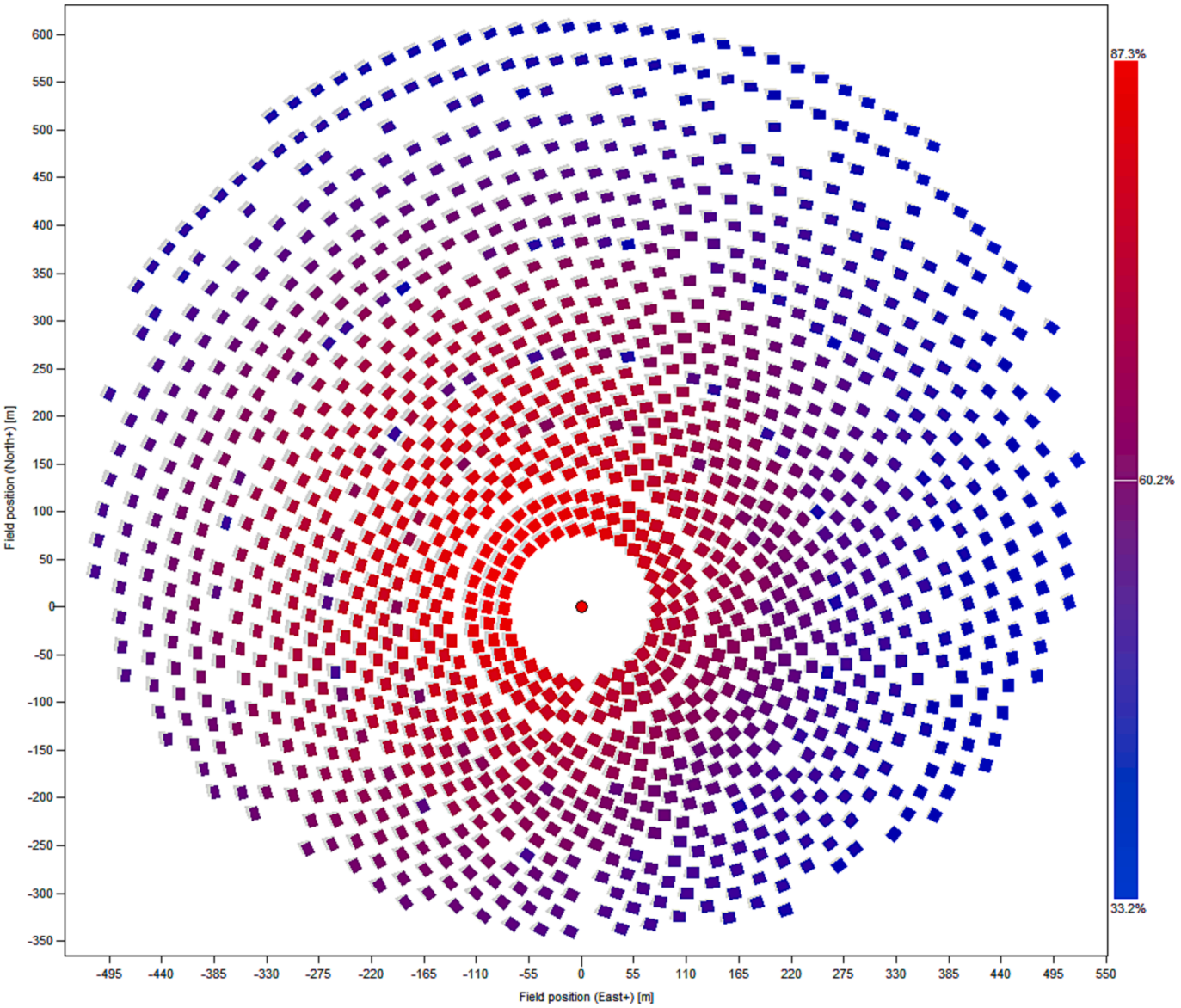

Fig. 7. Solar field layout and heliostat total efficiency calculated by SolarPilot.

Table 11
Geometrical and optical parameters of the heliostat field (default values in SolarPilot).

Heliostat structure width [m] × height [m]	12.2 × 12.2
N. of horizontal mirror facets	2
N. of vertical mirror facets	8
Surface slope error in X /Y [mrad]	1.53
Reflected beam error in X /Y [rad]	0.2
Mirror reflectivity	0.95

Table 12
Thermofluid-dynamic parameters of the microchannel receiver.

Useful thermal power [MW_{th}]	100.36
Fluid inlet/outlet temperature [°C]	510.4/700
Fluid inlet pressure [bar]	86.6
Pressure drop [bar]	4.075
Heat losses [MW_{th}]	5.473
Receiver thermal efficiency [%]	90.18
Receiver exergy efficiency [%]	57.55
Average fluid velocity in pass 1 [m/s]	15
Average convection heat transfer coefficient in pass 1 [$W\,m^{-2}\,°C^{-1}$]	$2.1{\cdot}10^3$
Average fluid velocity in pass 2 [m/s]	30
Average convection heat transfer coefficient in pass 2 [$W\,m^{-2}\,°C^{-1}$]	$4{\cdot}10^3$

compressor inlet temperature. Nonetheless, the power loss typically experienced in conventional gas turbines at high temperatures is mitigated here by the higher solar contribution.

The S-CO2 cycle is based on a recompression layout [7], but it has been modified in order to integrate both the high and intermediate-temperature thermal sources. Fig. 3a shows a classical s-CO2 recompression layout, where the sole thermal source is located upstream of the turbine (T), and there are two compressors and two recuperators. The components enclosed by a dashed line represent the equivalent single recuperator of a simple recuperated Brayton power cycle. In such a scheme, the main compressor (MC) operates close to the critical point. Different specific heat coefficients are exhibited for the high and low-pressure streams in the low-temperature zone of the equivalent recuperator (LTR in the recompression layout). Thus, different mass flow rates are established to balance the recuperator. Accordingly, the small mass flow rate (with higher specific heat) in the high-pressure stream requires an auxiliary compressor (AC) to manage the split mass flow rate

Table 13
Design point conditions for the heliostat field.

Location (latitude, longitude)	Seville (37.4 N, 5.9 W)
Day and hour	21st June, 12.00 solar hour
Direct Normal Irradiation, DNI [W/m^2]	950
Ambient temperature [°C]	25
Effective sky temperature [°C]	15
Wind velocity [m/s]	2

Table 14
Heliostat field geometry and performance.

Tower height [m]	108.21
Number of heliostats	1346
Optical efficiency [%]	77.31

by-passing the MC. The auxiliary compressor, with its suction upstream of the precooler (PC), increases the outlet temperature to a suitable value for mixing with the high-pressure stream leaving the LTR and before entering the high-temperature recuperator (HTR). In Fig. 3b, a modified recompression layout is shown, proposed in the current combined cycle. This modified layout does not need the AC, even though a lower mass flow rate in the high-pressure stream of the LTR is maintained to achieve a balanced heat exchanger. This is accomplished by splitting the mass flow rate after the compressor (C) and supplying heat from the intermediate-temperature (IT) source to the stream by-passing the LTR, before mixing it with the rest of the flow and entering the HTR. In some way, the IT source plays the role of the AC.

Fig. 3b shows another modification with respect to the classical recompression layout, enabling the integration of both high-temperature thermal sources (HTHR and CRS). This modification addresses the requirement of moderate pressure in the tubes at the HTHR and in the channels at the CRS, which is usually impossible if these sources are located upstream of the turbine. To solve this issue, the high-temperature (HT) thermal source has been moved downstream of the turbine, transferring the heat to the high-pressure side through the HTR. This arrangement has been previously proposed and analyzed by the authors, exploring different configuration options in CSP systems [16].

The HTHR, the ITHR and the LTHR are all cross-flow heat exchangers, where the streams flow unmixed. In all of them, the flue gases flow outside the tubes, while CO_2 (HTHR and ITHR) or the organic fluid (LTHR) flow inside them. The type of heat exchangers cannot withstand the high pressure required to maximize the S-CO2 cycle efficiency, typically around 300 bar. Therefore, the allocation of the HTHR and LTHR on the low-pressure side of the S-CO2 cycle allows for the combination of both restrictions: the use of conventional heat exchangers and the choice of the optimal pressure for the high-pressure side of the S-CO2 cycle. Such allocation also enables the use of CO_2 as the heat transfer fluid in the CRS, resulting in a direct cycle. As for the ITHR, since its thermal energy is supplied downstream of the compressor (C), an intermediate loop with CO_2 at low pressure is used. The heating loop heat exchanger (HLHX) is a printed circuit heat exchanger (PCHE) in order to withstand the pressure difference between the high pressure of the power cycle and the low pressure of the heating loop. Regarding the LTHR, the working fluid of the ORC directly flows inside the tubes as a recuperative transcritical cycle is selected, with 50 bar as the highest pressure. With two high-temperature thermal sources, two high-temperature recuperators are present: one for the flue gases (Gases High-Temperature Recueprator, G-HTR) and another for the solar source (Solar High-Temperautre Recuperator, S-HTR).

The central solar receiver is based on a microchannel configuration, which is particularly suitable for supercritical fluids such as CO_2. Specifically, this microchannel receiver combines two concepts [47]. From a macroscopic point of view, the receiver consists of a radial structure of several absorber panels, which converge on the central axis of the tower; this structure acts as a light-trapping geometry [48] that reduces heat loss by radiation, which can be significant at the actual elevated working temperatures (above 700 °C). From a microscopic point of view, the absorber panels consist of compact structures [49], whose compactness is gradually increased as the fluid is heated; this characteristic enhances the heat transfer to the working fluid, and thus the absorber cooling, only in the most thermally stressed parts of the absorber panel (higher concentrated solar radiation flux and/or hotter working fluid), without over penalizing its pressure drop. Fig. 4 shows a schematic of the microchannel receiver previously described and designed in this work. The compact structure considered is of the plain rectangular fin type with quadrangular channels. The fluid design velocities are 15 m/s in pass 1 and 30 m/s in pass 2. The receiver material is Alloy 617, which is recommended for compact heat exchangers working at the operating temperatures of the solar receiver [49]. The thermofluid-dynamic properties of CO_2 have been tabulated from the NIST database [50].

The solar subsystem consists of a circular heliostat field, which concentrates the solar radiation on the central receiver located at the top of the tower. The tower height has been determined according to the receiver's thermal power [14]. Once the characteristics of the receiver and the tower are established, the heliostat field is designed using the SolarPilot software [51]. For this design, the default heliostat size and optical parameters from SolarPilot have been used. In order to perform a more accurate calculation at the design point, the heliostat field obtained in SolarPilot is exported to Soltrace [52]. The calculation in Soltrace is based on the probabilistic Monte Carlo ray tracing method. This method involves simulating the trajectories of a large number of random sun rays (10^7 in this case), resulting in high accuracy. However, it is important to note that this approach is time-consuming and can only be applied to simulate particular moments. In this way, solar flux maps on the absorber panels and the solar field's optical efficiency, under design point conditions, are obtained using Soltrace.

2.2. Main hypothesis

The performance of the proposed system has been studied at the design point, established by maintaining constant inlet conditions of the air in the compressor of the gas turbine and of the cooling water in the condenser and precooler. ISO conditions [53] have been assumed for sizing purposes. The incoming working fluid temperature to the S-CO2 compressor and the ORC pump has been kept constant while varying the cooling water mass flow rate. Under these fixed conditions, the solar contribution characterized by the δ parameter has been varied from 0 to 100 %. Tables 1–4 show the boundary conditions at the different systems of the power plant.

In the combustion chamber of the gas turbine, a complete combustion process is assumed to take place, considering methane as fuel. Pressure drops are neglected [54]. Once inlet and outlet conditions at FGT have been established, the pressure ratio and the mass flow rate are calculated and kept constant.

In the S-CO2 system, the inlet temperature of the low-pressure streams to both HTR (points 8 and 12 in Fig. 1) is fixed, as well as the compressor inlet conditions and the compressor outlet pressure.

The selected working fluid for the ORC is R600 (n-butane), based on its excellent environmental properties (low GWP and null ODP). The operating pressures are also appropriate as the condensation pressure at 35 °C is 3.3 bar (above the atmospheric pressure) and the critical pressure is low, 39 bar. These characteristics allow for the design of a transcritical cycle at a moderately high pressure. Pressure drops are also neglected in this context [55].

2.3. Performance model

As mentioned earlier, while the cooling water temperature and ambient conditions are assumed to be constant, the solar radiation changes, which is quantified using the flue-gases split fraction, δ. The variation in the solar radiation involves significant changes in the

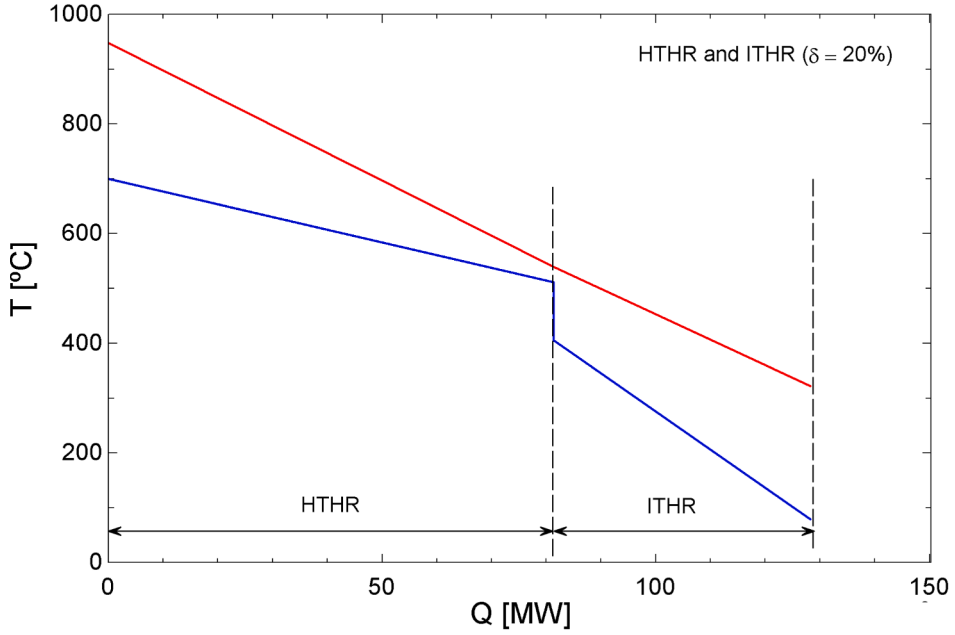

(a)

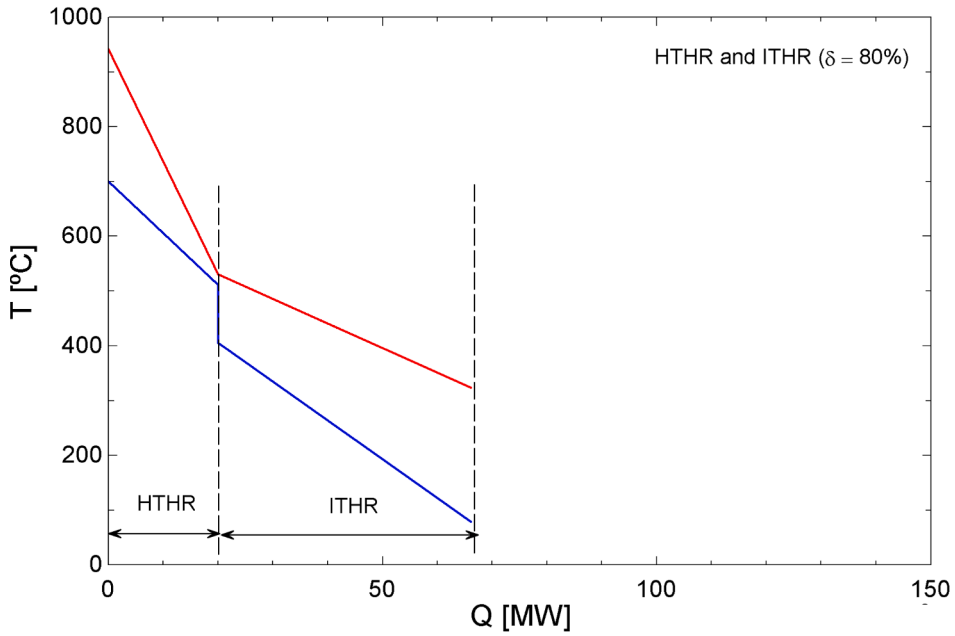

(b)

Fig. 8. Temperature profiles at high (HTHR) and intermediate (ITHR) temperature flue gases sources: (a) solar contribution of 20%; (b) solar contribution of 80%.

conditions at the two HTRs, with a higher duty occurring in the S-HTR for a larger solar contribution, as opposed to the G-HTR. Similar variations in conditions are observed at the HTHR and CRS of the S-CO2 power cycle. Alternatively, nearly constant conditions can be observed at the LTR, PC and HLHX heat exchangers, as well as in the CO_2 turbine and compressor. However, to be precise, slight variations can be expected due to the adjustment of the mass flow rate to maintain a temperature of 700 °C at points 8 or 12 (Fig. 2).

Compressors and pumps are assumed adiabatic and governed by Eq. (1), where w stands for specific work, h for enthalpy and η for isentropic efficiency. Subscripts i stands for "inlet", o for "outlet", c/p for "compressor/pump", and s represents the state with the same entropy as the inlet and the same pressure as the outlet. Turbines are also assumed adiabatic and governed by Eq. (2), where subscript T stands for "turbine", and the rest of notation is the same as in Eq. (1).

An energy balance in the heat exchangers is described by Eq. (3), where $\dot{m}$ stands for mass flow rate, $\dot{Q}$ for heat power exchanged, and the subscripts h and c stands for "hot" and "cold" respectively. Regarding the flow splitters, α is determined by balancing the LTR, whereas δ is imposed by the solar contribution.

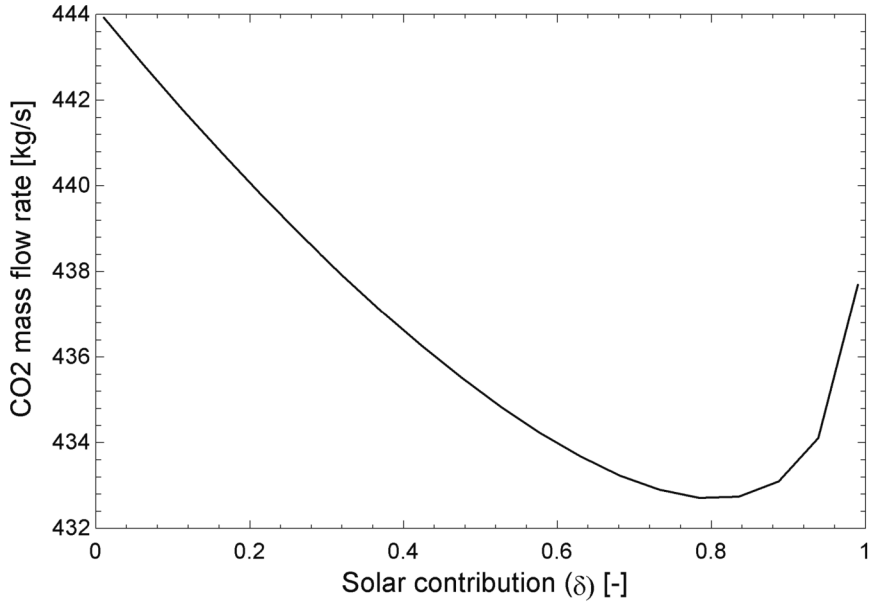

Fig. 9. Total CO_2 mass flow rate at no-split streams in the S-CO2 power cycle.

$$w_{c/p} = \frac{h_{o,s} - h_i}{\eta_{c/p}} \tag{1}$$

$$w_T = \eta_{c/p} \bullet \left(h_i - h_{o,s}\right) \tag{2}$$

$$\dot{Q} = \dot{m}_h \bullet (h_{hi} - h_{ho}) = \dot{m}_c \bullet (h_{co} - h_{ci}) \tag{3}$$

For the operation of the heat exchangers, that is, their performance when mass flow rates vary, the model of Patnode has been followed, along with the ε-NTU method [56]. The expressions have been taken from EES libraries [57], the simulation environment where the entire model has been implemented. Eq. (4) shows the relationship between the thermal conductance (*UA*) and the mass flow rates at design (subscript *N*) and off-design conditions. This model has been applied to the heat exchangers affected by the solar contributions: HTHR, G-HTR and S-HTR in the S-CO2 power cycle, G-REC in the gas turbine, and LTHR and O-REC in the ORC. Mass flow rates are nearly constant in the LTR, HLHX, and ITHR. Cooling water mass flow rates in the PC and COND vary to keep constant CO_2 and R600 temperatures, with minimal variation in their duties. In future analyses, when the plant operates under off-design conditions, the air mass flow rate will vary according to the ambient temperature [53]. This variation can be assessed using the thermal conductance model, similar to how it is done at the design point with the solar contribution.

$$\frac{UA}{UA_N} = \frac{\frac{1}{\dot{m}_{c,N}^{0.8}} + \frac{1}{\dot{m}_{h,N}^{0.8}}}{\frac{1}{\dot{m}_c^{0.8}} + \frac{1}{\dot{m}_h^{0.8}}} \tag{4}$$

Eqs. (5)–(7) calculate the net power of different systems: gas turbine (GT), Brayton supercritical CO2 (S-CO2) and ORC. Subscripts are defined in Fig. 2. Eq. (8) gives the combined cycle efficiency, taking into account the overall net power and the heat power input from both the combustion chamber (CCH) and the central receiver system (CRS). Finally, Eq. (9) gives the specific gas consumption of natural gas.

$$\dot{W}_{GT} = \dot{W}_{FGT} - \dot{W}_{AC} \tag{5}$$

$$\dot{W}_{S-CO2} = \dot{W}_T - \dot{W}_C - \dot{W}_{ITLP} \tag{6}$$

$$\dot{W}_{ORC} = \dot{W}_{O-T} - \dot{W}_{O-P} \tag{7}$$

$$\eta_{CC} = \frac{\dot{W}_{GT} + \dot{W}_{S-CO2} + \dot{W}_{ORC}}{\dot{Q}_{CCH} + \dot{Q}_{CRS}} \tag{8}$$

$$g = \frac{\dot{m}_{ng}}{\dot{W}_{GT} + \dot{W}_{S-CO2} + \dot{W}_{ORC}} \tag{9}$$

3. Results

3.1. Design point

The design point used to size all the components, except for the gas turbine recuperator, assumes a solar contribution of zero ($\delta = 0$). However, for the gas turbine recuperator, the condition is the opposite, and the maximum solar contribution ($\delta = 1$) is set to achieve the maximum duty of this particular heat exchanger. The design point conditions for the gas turbine components are summarised in Tables 5 and 6, while Tables 7–9 for each component of both bottoming cycles (S-CO2 and ORC).

Fig. 5 shows the p-h diagram of the S-CO2 power cycle and Fig. 6 represents the corresponding layout. To simplify the representation, parallel twin components (HTHR/CSR and G/S-HTR) have been condensed into single units. The main features of the S-CO2 power cycle can be observed.

One notable feature is that the compressor's energy consumption is significantly low compared to the turbine's production (hardly 14 % of self-consumption). As mentioned, the compressor suction (1 in Fig. 6) is close to the critical point, resulting in a reduced specific volume. This behavior is represented in Fig. 5 by the nearly vertical compressor line (1–2).

Another important aspect that can be observed is the balancing of the LTR through the use of different mass flow rates in each stream: line 2–10 is longer than line 8–9 in Fig. 5, due to the higher specific heat and, consequently, lower mass flow rate being directed through it.

In contrast to the traditional recompression layout (Fig. 3a), the auxiliary compressor in Fig. 5 is replaced by the heat input from the ITHR, which is transferred to the power cycle through the HLHX. The other novelty is the relocation of the high-temperature source (HTHR/CSR) downstream of the turbine, resulting in the line 6–7 in Fig. 5. The fluid then returns through the line 7–8 to transfer heat in the G/S-HTR.

The main geometrical parameters of the microchannel receiver are

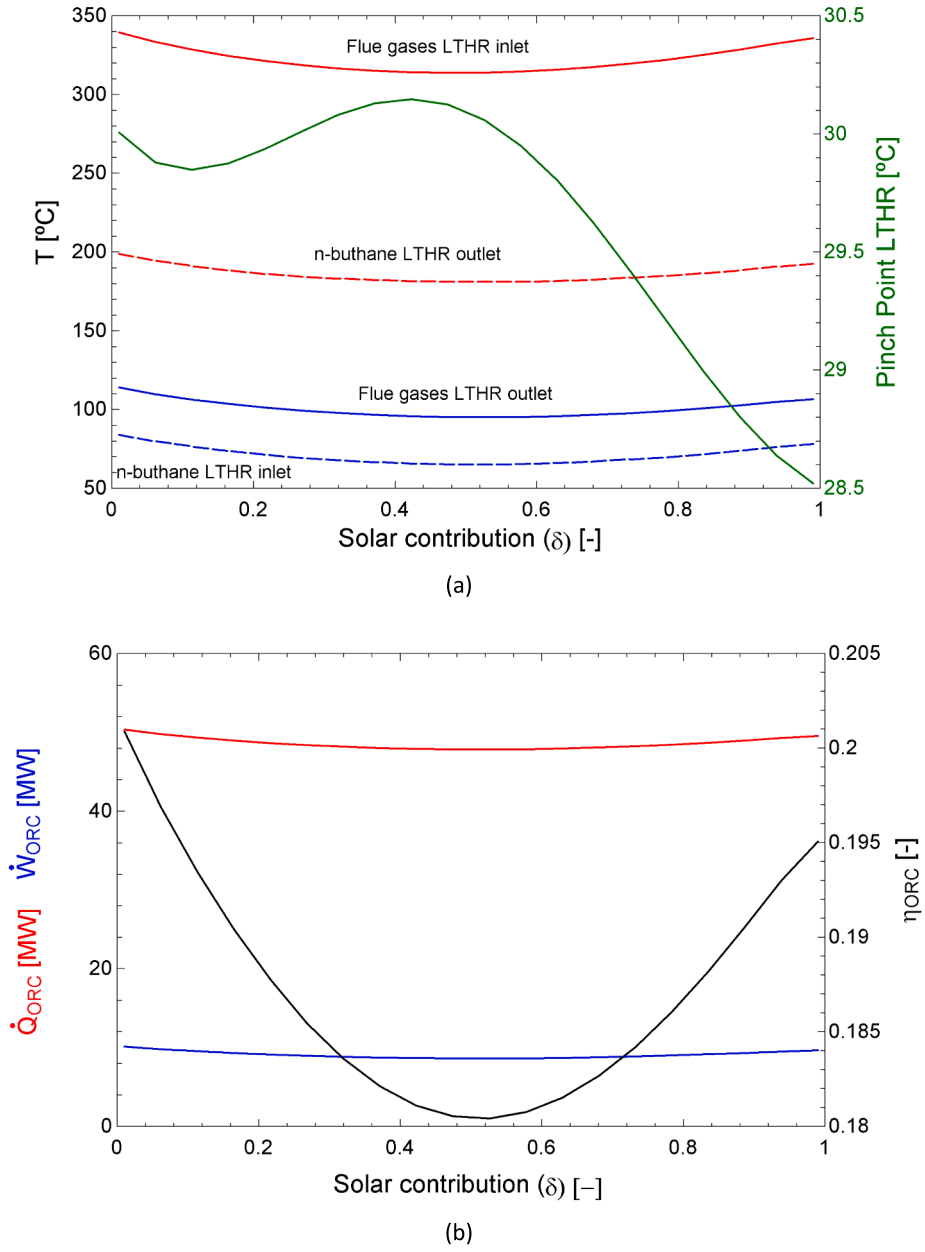

Fig. 10. (a) LTHR inlet and outlet temperatures; (b) energy conversion in the ORC.

summarized in Table 10. Both the number of converging absorber panels and their dimensions are the result of an optimisation process for exergy efficiency referred to the entire solar subsystem [22]. Fig. 7 shows the solar field layout and the heliostat efficiency calculated by SolarPilot and Table 11 lists the default geometrical and optical parameters considered by SolarPilot. Table 12 presents the thermo-hydraulic parameters of the microchannel receiver.

Seville has been selected as the location for sizing the solar field due to its favorable radiation conditions in Spain. Table 13 shows the design point conditions and Table 14 showcases the resulting heliostat field and its performance. However, it's important to note that the dimensions provided for the receiver and solar field are for illustrative purposes only. These simulations were obtained based on the design mass flow rate of flue gases from the gas turbine, which generates 102,785 kW at HTHR. The solar field has been sized in Seville to deliver this thermal power under the conditions outlined in Table 13. In future analysis, when assessing annual operation, the sizes of both solar field and receiver will be used to determine the actual heat power supplied by the solar system in response to instantaneous solar radiation.

3.2. Performance

Fig. 8 shows the effect of the solar contribution on the HTHR and ITHR. Fig. 8a represents a scenario with a low solar contribution ($\delta = 20$ %), where 80 % of the mass flow rate passing through the turbine FGT is directed to the HTHR. This configuration allows the HTHR to operate close to its design point, resulting in an exchange of approximately 80 MW of heat. Conversely, in Fig. 8b, with a high solar contribution ($\delta =$ 80 %), only 20 % of the mass flow rate crossing FGT is sent to the HTHR, leading to a reduced duty of 20 MW. The variation in the mass flow rate of the flue gases affects the thermal conductance, as described by Patnode [56]. This is evident in Fig. 8, where the log mean temperature difference is similar in both cases, but the amount of heat exchanged differs. In the case of the ITHR, no significant changes are appreciated

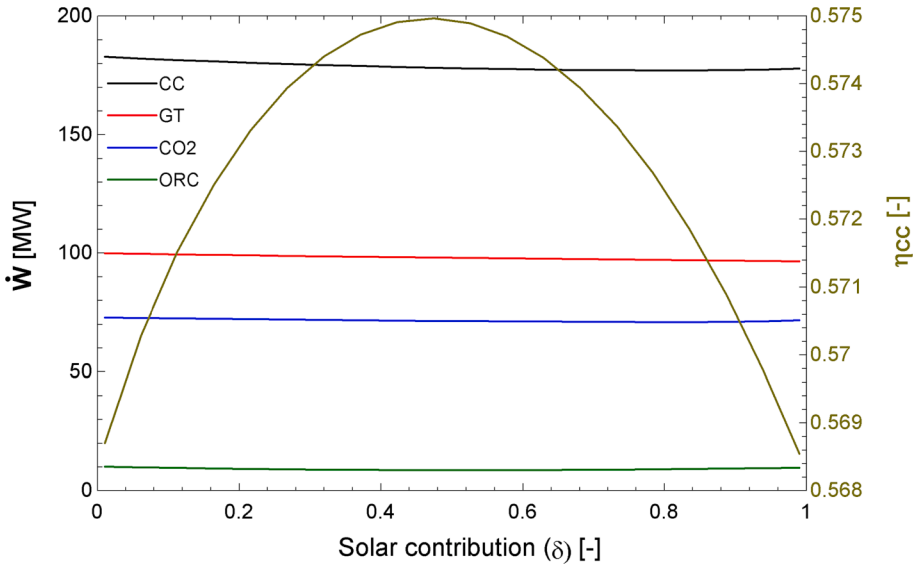

Fig. 11. Production of each power cycle and combined cycle efficiency.

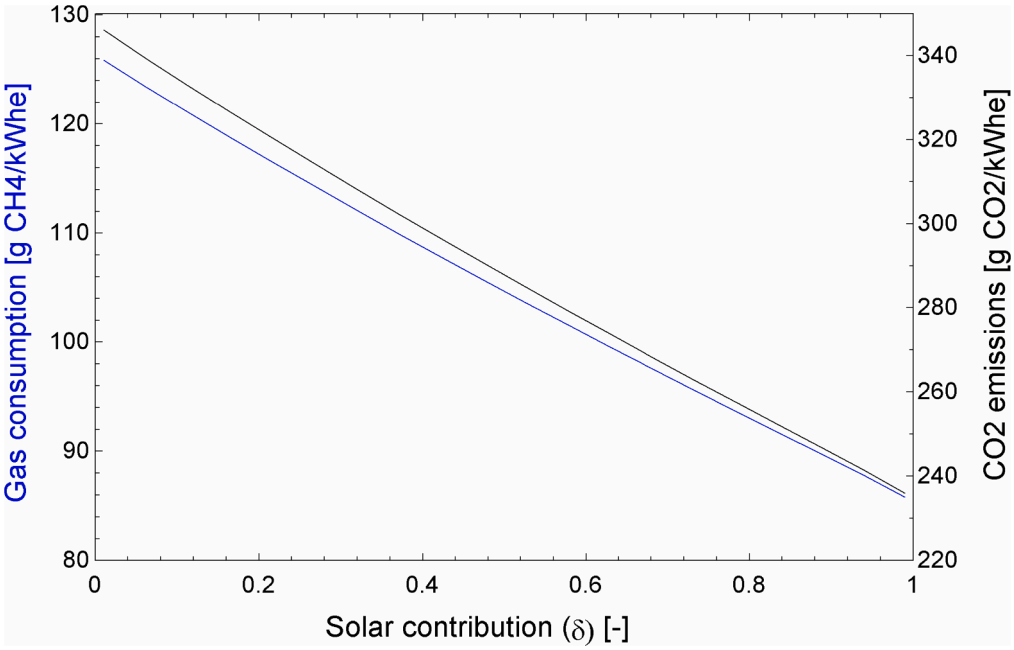

Fig. 12. Gas consumption and CO_2 emissions.

between Fig. 8a and 8b because all the mass flow rate of flue gases is mixed upstream, resulting in similar conditions. This behaviour aligns with the expected result that the mass flow rate of CO_2 remains nearly constant. Fig. 9 further confirms this, illustrating that the maximum variation in the mass flow rate of CO_2 is less than 2.7 %.

In relation to the ORC, Fig. 10a depicts the inlet and outlet temperatures of n-butane and flue gases in the LTHR as a function of the solar contribution. There is a relatively low variation in temperature, with a slightly higher variability observed in the flue-gases inlet temperature. At a 50 % solar contribution, the flue-gases inlet temperature reaches a minimum of 310 °C, while at 0 % and 100 % solar contribution, it reaches 340 °C (where no mixture occurs at point g5m). The curves of the temperature profiles are nearly parallel, indicating that the pinch point in the LTHR remains relatively constant, ranging from 28.5 °C to 30.2 °C. This behaviour is further demonstrated in Fig. 10b, where both the heat input and power output of the ORC are nearly constant. The efficiency of the ORC ranges between 18 % and 20 %, with the lowest efficiency occurring at 50 % solar contribution, corresponding to the minimum turbine inlet temperature. In order to avoid acid condensation in the stack, the ITHR has been sized to ensure a minimum flue-gases outlet temperature of 95 °C, as can be seen in Fig. 10a.

Fig. 11 shows the power produced by each cycle as a function of the solar contribution. A flat behaviour is observed, with an overall power production of 180 MWe and a global efficiency of 57.2 %. The ORC contributes only 5 % to the total power output, whereas both Brayton cycles sum up the remaining 95 % (56 % from the gas turbine and 39 % from the S-CO2 cycle). Taking into account the low contribution of the ORC to the overall power output, alternative uses for the intermediate-grade heat available in the flue gases at the LTHR (approximately 320 °C to 100 °C, and about 50 MWth) might be considered, depending on the location of the power plant. One possibility is the direct utilization of this heat for other applications. Another possibility would be to store

this heat and use it during short peak periods to boost power production.

Fig. 12 shows the performance associated with the natural gas. Its specific consumption decreases with the increase in solar contribution, although the system efficiency, as shown in Fig. 11, remains relatively constant. The efficiency depicted in Fig. 11 considers the overall heat input, including both natural gas and solar energy. The reduction in the consumption of natural gas leads to a decrease in carbon dioxide emissions. Without any solar contribution, the emissions are approximately 346 g CO_2/kWhe (126 g CH_4/kWh are consumed), while with the maximum solar contribution, the emissions decrease to around 236 g CO_2/kWhe (86 g CH_4/kWhe are consumed). Thus, a maximum reduction of 32 % in CO_2 emissions (related to natural gas consumption) can be achieved.

Fig. 12 might be surprising because even with full solar contribution, natural gas is consumed. This is due to the fact that the plant is an integration of a solar field with an advanced (S-CO2 instead of Rankine) combined cycle, with the gas turbine responsible for 56 % of the power output for any solar contribution under design conditions. The role of solar energy in this system is to reduce the gas consumption by enhancing the recuperative behaviour of the gas turbine when radiation increases. The role of natural gas is triple. Firstly, it reduces the size of the solar field (at maximum radiation, it produces 39 % of power output), contributing to the reduction of CAPEX. Secondly, it converts all solar radiation hours into equivalent hours, thus increasing the capacity factor. Finally, natural gas allows electricity production when there is no solar radiation without the need for thermal energy storage, which avoids potential issues with these systems.

4. Conclusions

A recuperative gas turbine combined with a Brayton supercritical CO_2 power cycle integrated with a central solar receiver system has been proposed. The solar contribution is integrated with flue gases from the gas turbine in order to obtain nearly constant power production at design conditions. This is achieved by employing a partially recuperated gas turbine, which enables the adjustment of the high-temperature flue gas mass flow rate supplied to the S-CO2 power cycle based on the solar contribution. When the solar contribution is low, a larger mass flow rate is directed to the S-CO2 power cycle, whereas a high solar contribution increases the duty of the gas turbine recuperator.

In this system, an intermediate-temperature heat recovery process replaces the auxiliary compressor used in conventional recompression S-CO2 schemes. Additionally, an ORC power cycle is used to take advantage of the low-temperature flue gases. A novel allocation of the heat input to the S-CO2 cycle enables the use of conventional cross-flow heat exchangers with circular-finned tubes in the flue-gases stream, while CO_2 serves as the heat transfer fluid in the solar receiver, thus constituting a direct cycle.

The integration of the central receiver system with the gas turbine avoids oversizing the solar field, and a reduction in the LCOE of the plant is expected. As thermal energy storage is not used, potential issues associated with this system, resulting from the high turbine inlet temperature required to increase efficiency, are avoided. Compared to a conventional CSP system, partial recuperation converts all solar hours into equivalent hours, thus increasing the capacity factor (under design conditions). The performance of the system at the gas turbine's design conditions has been assessed as a function of solar contribution. The overall power production of the system amounts to 180 MWe, achieving a global efficiency of 57.2 %. The ORC contributes only 5 % to the power output, whereas both Brayton cycles account for the remaining 95 % (56 % from the gas turbine and 39 % from the S-CO2 cycle). The system significantly reduces CO_2 emissions, up to 32 %, when the solar contribution reaches its maximum. Due to the relatively low contribution of the ORC to the overall power production, the recovered heat at the LTHR (50 MWth) could be directly utilized by nearby industries or stored to enhance power production during peak demands.

As the proposed system is an integrated solar combined cycle, the gas turbine is always in operation. Solar contribution reduces the gas consumption, with the maximum reduction occurring when power output is required in the absence of solar radiation (similar to the beahviour of a conventional combined cycle). In future work, annual performance will be obtained by considering actual variations in radiation and ambient temperature. In the current analysis, ambient conditions have been maintained constant (design conditions), while the recuperation in the gas turbine was varied.

Declaration of Competing Interest

The authors declare that they have no known competing financial interests or personal relationships that could have appeared to influence the work reported in this paper.

Acknowledgements

This work has been supported by the Spanish Ministry of Science and Innovation through the PID2019-110283RB-C33 project.

References

[1] L. Crespo, CSP Markets and Projects. Oral communication at SolarPACES 2019, 2019.
[2] International Energy Agency, Projected costs of generating electricity, IEA & NEA, 2020.
[3] M.d. Tasbirul, N. Huda, A.B. Abdullah, R. Saidur, A comprehensive review of state-of-the-art concentrating solar power (CSP) technologies: current status and research trends, Renew. Sustain. Energy Rev. 91 (2018) 987–1018.
[4] IRENA, Renewable power generation costs in 2019, Tech. Rep., International Renewable Energy Agency, Abu Dhabi, 2020, p. 144.
[5] US Department of Energy, SunShot Vision Study. Chap. 5. Feb. 2012, p. 115.
[6] M. Mehos, C. Turchi, J. Vidal, M. Wagner, Z. Ma, C. Ho, et al., Concentrating Solar Power Gen3 Demonstration Roadmap. NREL, NREL/TP-5500-67464, 2017.
[7] V. Dostal, A Supercritical Carbon Dioxide Cycle for Next Generation Nuclear Reactors, Institute of Technology, Massachusetts, 2004. Doctoral Thesis.
[8] K. Sajwan, M. Sharma, A.K. Shukla, Distrib. Gener. Alter. Energy J. 35 (2021) 111–138.
[9] C.S. Turchi, Z. Ma, J. Dyreby, Supercritical carbon dioxide power cycle configurations for use in concentrating solar power systems, in: Proceedings of the ASME Turbo Expo 2012, American Society of Mechanical Engineers, Copenhagen, Denmark, 2012, pp. 967–973.
[10] C. Turchi, 10 MW Supercritical CO_2 Turbine Test, National Renewable Energy Laboratory, 2014, (No. DE-EE0002589).
[11] F. Crespi, G. Gavagnin, D. Sánchez, G.S. Martínez, Supercritical carbon dioxide cycles for power generation: a review, Appl. Energy 195 (2017) 152–183.
[12] K. Wang, Y.-L. He, H.-H. Zhu, Integration between supercritical CO 2 Brayton cycles and molten salt solar power towers: a review and a comprehensive comparison of different cycle layouts, Appl. Energy 195 (2017) 819–836.
[13] B.D. Iverson, T.M. Conboy, J.J. Pasch, A.M. Kruizenga, Supercritical CO_2 Brayton cycles for solar-thermal energy, Appl. Energy 111 (2013) 957–970.
[14] M.J. Montes, J.I. Linares, R. Barbero, A. Rovira, Proposal of a new design of source heat exchanger for the technical feasibility of solar thermal plants coupled to supercritical power cycles, Sol. Energy 211 (2020) 1027–1041.
[15] M.J. Montes, J.I. Linares, R. Barbero, B.Y. Moratilla, Optimization of a new design of molten salt-to-CO_2 heat exchanger using exergy destruction minimization, Entropy 22 (2020) 883.
[16] J.I. Linares, M.J. Montes, A. Cantizano, M.C. Sánchez, A novel supercritical CO_2 recompression Brayton power cycle for power tower concentrating solar plants, Appl. Energy 263 (2020), 114644.
[17] E. Johnson, L. Bates, A. Dower, P.C. Bueno, R. Anderson, Thermal energy storage with supercritical carbon dioxide in a packed bed: modeling charge-discharge cycles, J. Supercrit. Fluids 137 (2018) 57–65.
[18] Q.i. Li, G. Flamant, X. Yuan, P. Neveu, L. Luo, Compact heat exchangers: a review and future applications for a new generation of high temperature solar receivers, Renew. Sustain. Energy Rev. 15 (9) (2011) 4855–4875.
[19] C.K. Ho, B.D. Iverson, Review of high-temperature central receiver designs for concentrating solar power, Renew. Sustain. Energy Rev. 29 (2014) 835–846.
[20] S.M. Besarati, D. Yogi Goswami, E.K. Stefanakos, Development of a solar receiver based on compact heat exchanger technology for supercritical carbon dioxide power cycles, J. Sol. Energy Eng. 137 (2015), 031018.
[21] S.D. Sullivan, J. Kesseli, J. Nash, J. Farias, D. Kesseli, W. Caruso, High-Efficiency Low-Cost Solar Receiver for Use Ina a Supercritical CO_2 Recompression Cycle (No. DOE-BRAYTON-0005799, 1333813), 2016.
[22] M.J. Montes, R. Guédez, D. D'Souza, J.I. Linares, J. González-Aguilar, M. Romero, Proposal of a new design of central solar receiver for pressurised gases and supercritical fluids, Int. J. Therm. Sci. 194 (2023) 108586.

[23] M.J. Montes, R. Guedez, J.I. Linares, M.A. Reyes-Belmonte, Advances in solar thermal power plants based on pressurised central receivers and supercritical power cycles, Energ. Conver. Manage. 293 (2023) 117454.
[24] J. Song, X. Li, X. Ren, C. Gu, Performance analysis and parametric optimization of supercritical carbon dioxide (S-CO2) cycle with bottoming organic Rankine cycle (ORC), Energy 143 (2018) 406–416.
[25] H. Singh, R.S. Mishra, Performance analysis of solar parabolic trough collectors driven combined supercritical CO_2 and organic Rankine cycle, Eng. Sci. Technol. Int. J. 21 (3) (2018) 451–464.
[26] S. Hou, S. Cao, L. Yu, Y. Zhou, Y. Wu, F. Zhang, Performance optimization of combined supercritical CO_2 recompression cycle and regenerative organic Rankine cycle using zeotropic mixture fluid, Energ. Conver. Manage. 166 (2018) 187–200.
[27] F. Rovense, M.A. Reyes-Belmonte, J. González-Aguilar, M. Amelio, S. Bova, M. Romero, Flexible electricity dispatch for CSP plant using un-fired closed air Brayton cycle with particles based thermal energy storage system, Energy 173 (2019) 971–984.
[28] W.-D. Steinmann, Thermal energy storage systems for concentrating solar power (CSP) technology. In Advances in thermal energy storage systems, 2015, pp. 511–531.
[29] K.M. Powell, K. Rashid, K. Ellingwood, J. Tuttle, B.D. Iverson, Hybrid concentrated solar thermal power systems: a review, Renew. Sustain. Energy Rev. 80 (2017) 215–237.
[30] G. Zhu, T. Neises, C. Turchi, R. Bedilion, Thermodynamic evaluation of solar integration into a natural gas combined cycle power plant, Renew. Energy 74 (2015) 815–824.
[31] Y. Allani, D. Favrat, M.R. Spakovsky, CO_2 mitigation through the use of hybrid solar-combined cycles, Energ. Conver. Manage. 38 (1997) S661–S667.
[32] M. Kane, D. Favrat, K. Ziegler, Y. Allani, Thermoeconomic analysis of advanced solar-Fossil combined power plants, Int. J. Thermodyn. 3 (2000) 191–198.
[33] J. Dersch, M. Geyer, U. Herrmann, S.A. Jones, B. Kelly, R. Kistner, W. Ortmanns, R. Pitz-Paal, H. Price, Trough integration into power plants—A study on the performance and economy of integrated solar combined cycle systems, Energy 29 (5) (2004) 947–959.
[34] G. Franchini, A. Perdichizzi, S. Ravelli, G. Barigozzi, A comparative study between parabolic trough and solar tower technologies in solar Rankine cycle and integrated solar combined cycle plants, Sol. Energy 98 (2013) 302–314.
[35] M. Sharma, O. Singh, Energy and exergy investigations upon tri-generation based combined cooling, heating, and power (CCHP) system for community applications. In Proceedings of the ASME 2017 Gas Turbine India Conference, Bangalore, India, December 7-8, GTINDIA2017-4559, 2017.
[36] M.A. Reyes-Belmonte, A. Sebastian, J. Spelling, M. Romero, J. Gonzalez-Aguilar, Annual performance of subcritical Rankine cycle coupled to an innovative particle receiver solar power plant, Renew. Energy 130 (2019) 786–795.
[37] A. Rovira, R. Barbero, M.J. Montes, R. Abbas, F. Varela, Analysis and comparison of integrated solar combined cycles using parabolic troughs and linear Fresnel reflectors as concentrating systems, Appl. Energy 162 (2016) 990–1000.
[38] N. Khandelwal, M. Sharma, O. Singh, A.K. Shukla, Comparative evaluation of Integrated Solar combined cycle plant with cascade thermal storage system for different heat transfer fluids, J. Clean. Prod. 353 (2022) 131519.
[39] M. Amelio, V. Ferraro, V. Marinelli, A. Summaria, An evaluation of the performance of an integrated solar combined cycle plant provided with air-linear parabolic collectors, Energy 69 (2014) 742–748.
[40] L. Duan, W. Qu, S. Jia, T. Feng, Study on the integration characteristics of a novel integrated solar combined cycle system, Energy 130 (2017) 351–364.
[41] E. Okoroigwe, A. Madhlopa, An integrated combined cycle system driven by a solar tower: a review, Renew. Sustain. Energy Rev. 57 (2016) 337–350.
[42] A. Franco, C. Casarosa, On some perspectives for increasing the efficiency of combined cycle power plants, Appl. Therm. Eng. 22 (13) (2002) 1501–1518.
[43] T. Liu, G. Zhang, Y. Li, Y. Yang, Performance analysis of partially recuperative gas turbine combined cycle under off-design conditions, Energ. Conver. Manage. 162 (2018) 55–65.
[44] A. Rovira, M. Muñoz, C. Sánchez, R. Barbero, Advanced thermodynamic cycles for finite heat sources: proposals for closed and open heat sources applications, Appl. Therm. Eng. 167 (2020) 114805.
[45] A. Rovira, R. Abbas, J.I. Linares, M. Muñoz, M.J. Montes, AdInCCSol: advanced integration of combined cycles in solar thermal power plants. Oral communications at SolarPACES 2021, 2021.
[46] A. Rovira, M. Muñoz, C. Sánchez, R. Barbero, Advanced thermodynamical cycles for finite heat sources: proposals for closed and open heat sources applications, Appl. Therm. Eng. 167 (2020), 114805.
[47] M.J. Montes, A. Rovira, J. González-Aguilar, M. Romero, Spanish Patent Application No. 202131189, 2021.
[48] C.K. Ho, J.M. Christian, J.D. Ortega, J. Yellowhair, M.J. Mosquera, C.E. Andraka, Reduction of radiative heat losses for solar thermal receivers, in: Proceedings of the SPIE Optics+Photonics Solar Energy+Technology High and Low Concentrator Systems for Solar Energy Applications IX, San Diego, August 17–21, 2014, 2014.
[49] Q. Li, G. Flamant, X. Yuan, P. Neveu, L. Luo, Compact heat exchangers: a review and future applications for a new generation of high temperature solar receivers, Renew. Sustain. Energy Rev. 15 (2011) 4855–4875.
[50] NIST database https://webbook.nist.gov/chemistry/, doi: 10.18434/T4D303.
[51] M.J. Wagner, T. Wendelin, SolarPILOT: a power tower solar field layout and characterization tool, Sol. Energy 171 (2018) 185–196.
[52] T. Wendelin, SolTRACE: a new optical modeling tool for concentrating solar optics, in: Proceedings of the ISEC 2003: International Solar Energy Conference, 15-18 March 2003, Kohala Coast, Hawaii. New York: American Society of Mechanical Engineers, pp. 253-260; NREL Report No. CP-550-32866, 2003.
[53] F.J. Brooks, GE Gas Turbine Performance Characteristics (GER-3567H). GE Power Systems, Available on: https://www.ge.com/content/dam/gepower-new/global/en_US/downloads/gas-new-site/resources/reference/ger-3567h-ge-gas-turbine-performance-characteristics.pdf (Accesed on 09 July 2023).
[54] H.I.H. Saravanamuttoo, G.F.G. Rogers, H. Cohen, P.V. Straznicky, A.C. Nix, Gas Turbine Theory, seventh ed., Pearson, Harlow (England), 2017.
[55] S. Lecompte, H. Huisseune, M. Broek, B. Vanslambrouck, M.D. Paepe, Review of organic Rankine cycle (ORC) architextures for waste heat recovery, Renew. Sustain. Energy Rev. 47 (2015) 448–461.
[56] A.M. Patnode, Simulation and Performance Evaluation of Parabolic Trough Solar Power Plants, University of Wisconsin-Madison: College of Engineering, Madison, 2006. Master Thesis.
[57] S. Klein, G. Nellis, Mastering EES, F-Chart Software, Madison (Wisconsin), 2021.